Transactions of NAMP 23, (2025) 117-126

Transactions of
The Nigerian Association of
Mathematical Physics
Journal homepage: https://nampjournals.org.ng

INVESTIGATION OF CRITICAL FACTORS AFFECTING PRESSURE DISTRIBUTION OF A HORIZONTAL WELL NEAR A SEALING OIL RESERVOIR EXTERNAL BOUNDARY

M. U. AKONGWALE[1], C. OKON[2] AND E.S. ADEWOLE[3]
[1,2]*Department of Petroleum Engineering, University of Calabar, Nigeria*
[3]*Department of Petroleum Engineering, University of Benin, Benin City, Nigeria*

ARTICLE INFO

Article history:
Received xxxxx
Revised xxxxx
Accepted xxxxx
Available online xxxxx

Keywords:
Horizontal Well,
Pressure Distribution,
Sealing Boundary.

ABSTRACT

Horizontal wells enhance reservoir contact and productivity, but display complex pressure behaviour due to reservoir boundary effects, well design, reservoir fluid and wellbore conditions. This paper investigates the factors affecting pressure distribution in a horizontal well located near a sealing boundary, with emphasis on the implications of well design and key reservoir parameters on well performance. The principle of superposition is utilized to compute dimensionless pressure and pressure derivatives of horizontal well near a sealing boundary. Object well distances from the sealing boundary, well skin and storage were considered. Reservoir anisotropy is not considered.

Results show that critical factors affecting horizontal well performance are dimensionless wellbore radius, horizontal well length, wellbore skin and storage factor. Furthermore, two characteristic pressure gradients are observable: infinite-acting flow and boundary dominated regime with a slope of 2.3026 per cycle.

INTRODUCTION

Horizontal wells are widely adopted in petroleum engineering to maximize contact between the wellbore and the reservoir pay zone, boosting production and reservoir recovery however in reservoirs bounded by sealing boundaries, such as an impermeable fault or an aquifer, the pressure distribution around a horizontal well exhibits distinctive behavior due to boundary-induced flow restrictions and reservoir geometry constraints. Analytical models based on line-Source and Green's functions have demonstrated how constant-pressure top and bottom boundaries alter pressure and pressure derivative evolution over time. In anisotropic reservoirs, particularly those with sealed boundaries at the base or edges, well-test analysis of horizontal wells reveals boundary-induced late-time pseudo-steady flow regimes and anisotropy-sensitive diagnostic signatures [5],

*Corresponding author: M. U. AKONGWALE
E-mail address: mercyunimashi@gmail.com
https://doi.org/10.60787/tnamp.v23.629

however, the specific influence of external sealing boundaries on pressure distribution patterns and pressure derivative behavior has not been comprehensively investigated in the literature.

Horizontal wells often enhance recovery by exposing more reservoir area to the wellbore. However, their pressure-transient response is more complex than vertical wells, exhibiting bilinear, linear, and boundary-dominated flow regimes [6],[7],[8]. Sealing faults or no-flow boundaries impose a constant-pressure or zero-flux condition that alters the late-time pressure behavior. When a horizontal well lies near a sealing boundary, type-curve slopes change, and boundary-dominated flow appears earlier [1],[8]. Variations in reservoir properties, including permeability and porosity, affect fluid flow and pressure propagation. Existing studies address bounded reservoirs but often oversimplify by assuming constant pressure conditions or focusing on well test analysis rather than pressure field modeling [3],[5]. The primary aim of this study is to analytically examine pressure distribution in a horizontal well near a sealing oil reservoir boundary under varying critical parameters.

PHYSICAL RESERVOIR SYSTEM MODEL DESCRIPTION

Figure 1 shows a horizontal well of dimensionless radius, r_{wD}, and dimensionless length, L_D, located at a dimensionless distance, d, away from a sealing boundary. Dimensionless pressures and dimensionless pressure derivatives of the well are computed for different well designs and completion, to investigate the critical factors that affect well performance in real time when the well is placed on oil production. The sealing acts as a plane mirror, which, therefore, reproduces the image of the object horizontal well in exactly the same way as itself. Hence, by the principle of lateral inversion, the image well is also located at a dimensionless distance, d, behind the sealing boundary. This means that the object and image wells are separated by dimensionless distance 2d. During oil production from the object well, transient pressure, which is like mechanical waves, produce echoes (reversal of transient waves), whose strength as felt in the object well, depends on the distance of the sealing boundary. The total dimensionless pressure drop in the object well is calculated for different well designs, completion, and distance from the sealing boundary.

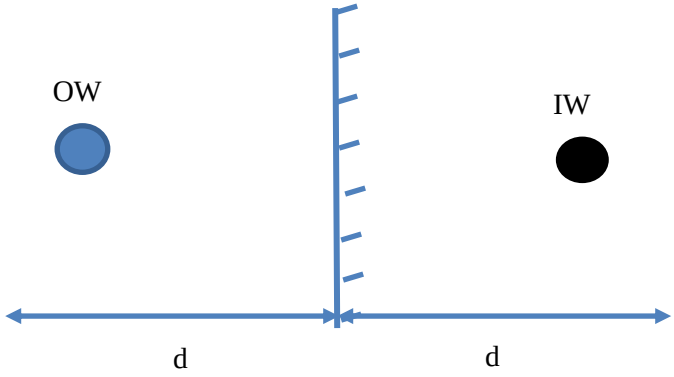

Figure 1: Reservoir System Physical Model

MATHEMATICAL MODEL DESCRIPTION

From the physical model description, the total dimensionless pressure drop in the object well is derived using the principle of superposition as the sum of dimensionless pressure in the object well due to flow in the object well and the dimensionless pressure drop in the object well due to flow in the image well. That is,

$$p_{DOW,T} = p_{OW,OW} + p_{DOW,IW} \quad (1)$$

Using mathematical expressions [2],[4] Equation 1 is written as

$$p_{Dow,T} = -\frac{\alpha}{4LD}\,Ei\left(-\frac{r_{wD}^2}{\frac{4tD}{cD}}\right) + s - \frac{\propto}{4LD}\,Ei\left(-\frac{(2d)^2}{4tD}\right). \quad (2)$$

where $\alpha = 2$, for an infinite conductivity case. It can be shown that at long dimensionless times, where the arguments of the Ei functions become less or equal to 0.01, Equation 2 becomes

$$p_{Dow,T} = -\frac{2.3026\alpha}{4LD}\log\left(\frac{1{,}781r_{wD}^2}{\frac{4tD}{cD}}\right) + s - \frac{2.3026\alpha}{4LD}\log\left(\frac{1.781(2d)^2}{4tD}\right) \quad (3)$$

Using the laws of logarithms, Equation can be written as

$$p_{Dow,T} = -\frac{2x2.3026\alpha}{4LD}\log\left(\frac{1.781dr_{wD}}{\frac{4tD}{cD}}\right) + s \quad (4)$$

The dimensionless pressure derivative is expressed as

$$p_D^{'} = t_D\frac{\partial p_D}{\partial t_D} \quad (5)$$

The dimensionless pressure gradient per cycle is

$$\frac{\partial p_{Dow,T}}{\partial t_D} = \frac{2.3026\propto}{4L_D}\left[\exp\left(-\frac{r_{wD}^2}{4\frac{t_D}{c_D}}\right) + \exp\left(-\frac{(2d)^2}{4t_D}\right)\right] \quad (6)$$

Therefore, at all dimensionless times, dimensionless pressure derivative using Equation 3 is

$$p_{Dow,T}^{'} = \frac{\propto}{4L_D}\exp\left(-\frac{r_{wD}^2}{\frac{4tD}{cD}}\right) + \frac{\propto}{4L_D}\exp\left(-\frac{(2d)^2}{4t_D}\right) \quad (7)$$

At very late dimensionless times, dimensionless pressure gradient using Equation 4 is derived as

$$\frac{\partial p_D}{\partial t_D} = \frac{2.3026}{L_D} \quad (8)$$

A straight sealing boundary is akin to two plane mirrors inclined at an angle of 180^0. according to Reference [9], the number of images formed due to such inclination should be 1. Results obtained will be interpreted to prove that the number of images is 1, using dimensionless pressure gradients and dimensionless pressure derivatives results. All equations are implemented in Microsoft Excel spreadsheet and verified with MATLAB scripts. Using identical reservoir, well boundary parameters, dimensionless pressure derivative responses were generated over the same dimensionless time range. The results were compared from both platforms numerically and graphically, thereby validating the correctness and accuracy of the analytical formulations.

RESULTS AND DISCUSSION

Reservoir system parameters are assumed and the equations above are used to calculate dimensionless pressure, dimensionless pressure derivative and dimensionless pressure gradients. To understand effect of each parameter on overall result, sets of parameters are kept constant while one is varied. Reservoir system parameters considered are object well dimensionless distance from the sealing boundary, well design and well completion parameters. Results obtained are shown in Tables 1 to 9 and Figures 2 to 9.

Table 1: Dimensionless Pressure for c_D=0.01, L_D= 1, r_{wD}=0.0005, s = 0

t_D	d=0.3	d=1.2	d=3.0	d=4.5
0.01	8.0054	8.0054	8.0054	8.0054
0.1	9.2868	9.1567	9.1567	9.1567
1	13.3305	12.2092	11.5894	11.4829
10	15.8290	14.4494	13.5700	13.2169
100	18.1312	16.7456	15.8331	15.4332
1000	20.4337	19.0475	18.1316	17.7267

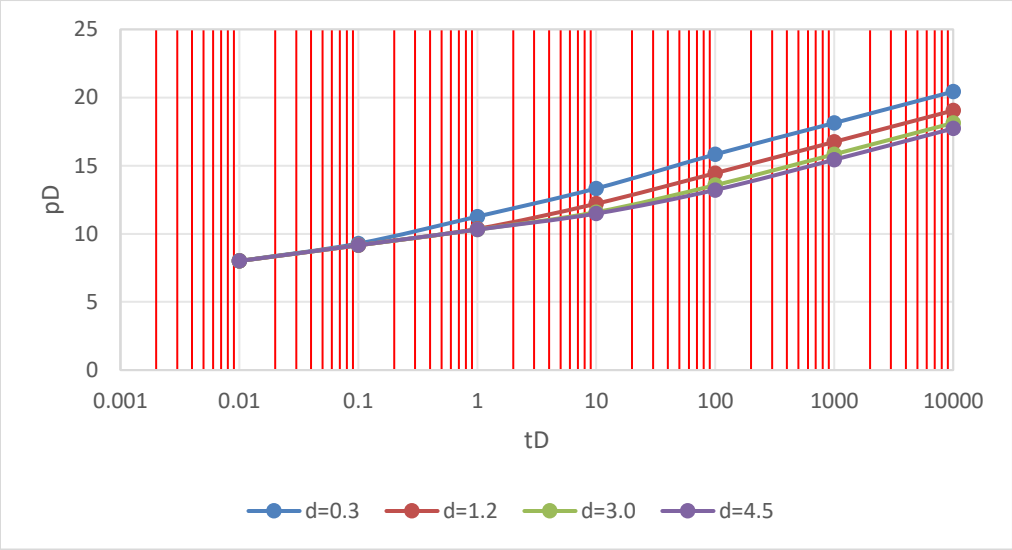

Figure 2: Plot of Dimensionless Pressure versus Dimensionless Time for various distances d from the sealing boundary with c_D=0.01, L_D= 1, r_{wD}=0.0005, s = 0

Table 2: Dimensionless Pressure for c_D=0.001, L_D= 1, r_{wD}=0.0005, s = 1

t_D	d=0.3	d=1.2	d=3.0	d=4.5
0.01	9.0054	9.0054	9.0054	9.0054
0.1	10.2868	10.1567	10.1567	10.1567
1	14.5305	13.2092	12.5894	12.4829
10	16.8290	15.4494	14.5700	14.2169
100	19.1312	17.7456	16.8331	16.4332
1000	21.4337	20.0475	19.13.16	18.7267

Table 3: Dimensionless Pressure for c_D=0.01, L_D= 1, r_{wD}=0.0005, s = +5

t_D	d=0.3	d=1.2	d=3.0	d=4.5
0.01	13.0054	13.00544	13.0054	13.0054
0.1	14.2868	14.1567	14.1567	14.1567
1	18.5304	17.2092	16.5894	16.4829
10	20.8290	19.4494	18.5700	18.2169
100	23.1312	21.7456	20.8331	20.4332
1000	25.4337	24.0475	23.1316	22.7267

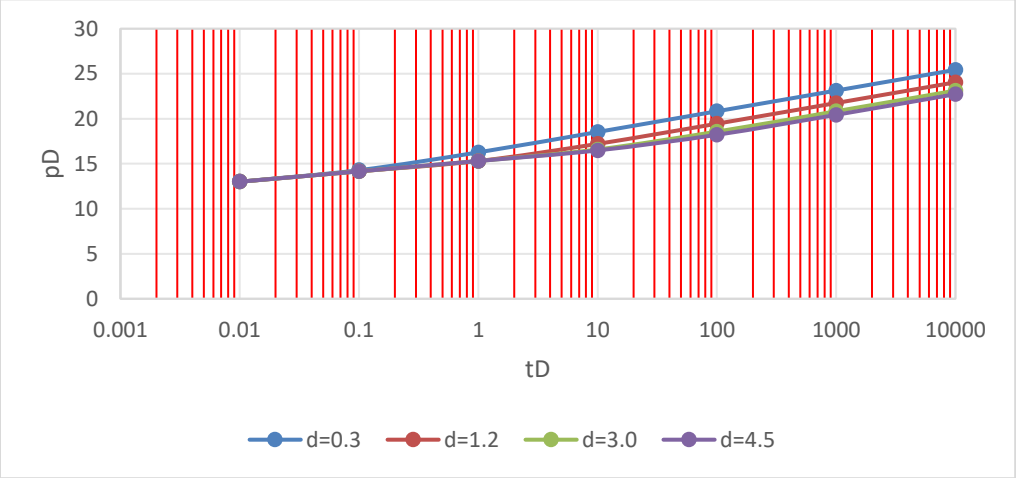

Figure 3: Dimensionless Pressure for c_D=0.01, L_D= 1, r_{wD}=0.0005, s = +5

Table 4: Dimensionless Pressure for c_D=0.01, L_D= 1, r_{wD}=0.001, s = -1

t_D	d=0.3	d=1.2	d=3.0	d=4.5
0.01	6.3123	6.3123	6.3123	6.3123
0.1	7.5937	7.4636	7.4636	7.4636
1	11.8373	10.5160	9.3963	9.7898
10	14.1359	12.7563	11.8768	11.5237
100	16.4380	15.0524	14.1399	13.7400
1000	18.7406	17.3544	16.4385	16.0336

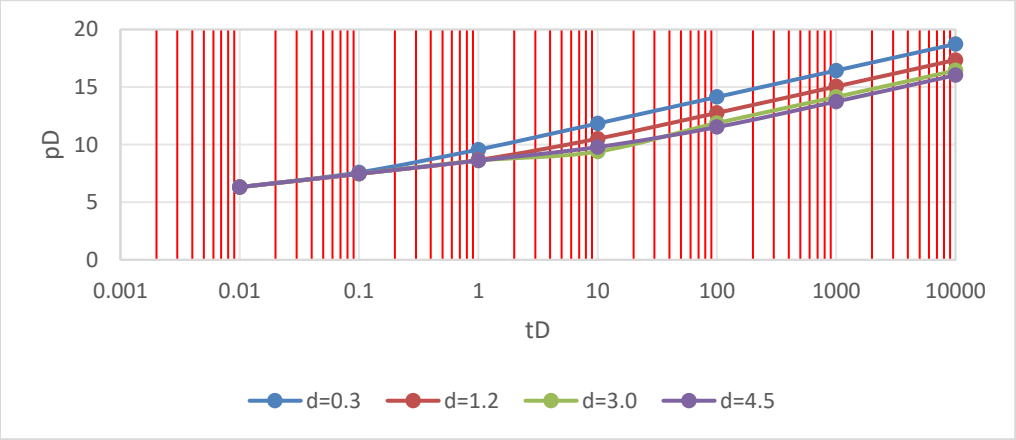

Figure 4: Dimensionless Pressure for c_D=0.01, L_D= 1, r_{wD}=0.001, s = -1

Table 5: Dimensionless Pressure for c_D=0.01, L_D= 10, r_{wD}=0.0005, s = -1

t_D	d=0.3	d=1.2	d=3.0	d=4.5
0.01	0.0000	0.0000	0.0000	0.0000
0.1	0.1224	0.0000	0.0000	0.0000
1	0.3530	0.2209	0.1589	0.1483
10	0.5829	0.4442	0.3570	0.3217
100	0.8131	0.6745	0.5829	0.5423
1000	1.0434	0.9048	0.8131	0.7726

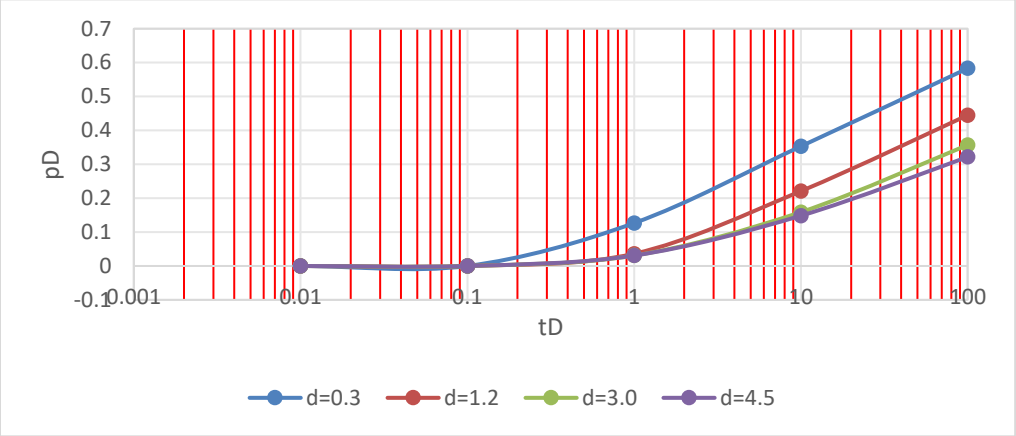

Figure 5: Dimensionless Pressure for c_D=0.01, L_D= 10, r_{wD}=0.0005, s = -1

Table 6: Dimensionless Pressure vs Time for c_D=0.01, L_D= 1, r_{wD}=0.0005, s = -1

t_D	d = 0.3	d = 1.2	d = 3.0	d = 4.5
0.01	7.0054	7.0054	7.0054	7.0054
0.1	8.2868	8.1567	8.1567	8.1567
1	12.5304	11.2092	10.5894	10.4829
10	14.8290	13.4494	12.5699	12.2169
100	17.1312	15.7456	14.8331	14.4332
1000	19.43375	18.0475	17.1316	16.7267

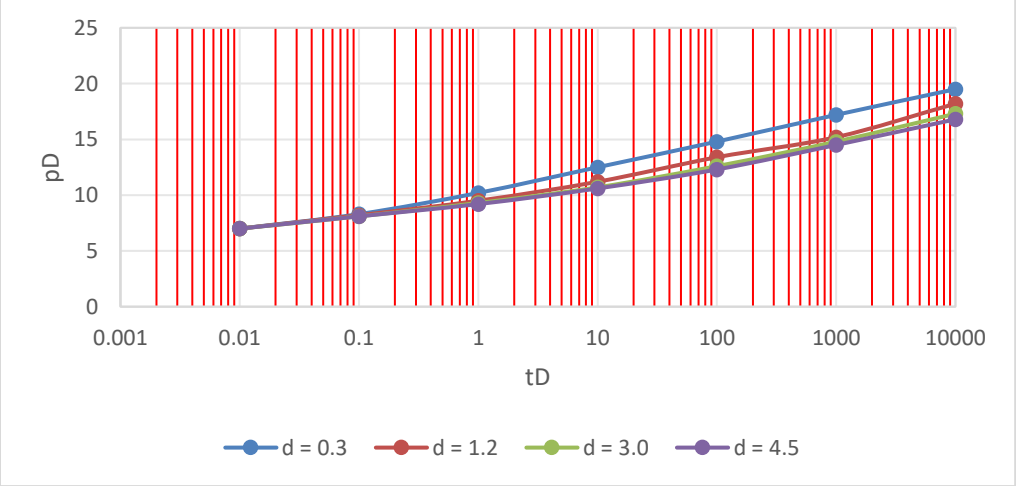

Figure 6: Dimensionless Pressure Derivative vs Time for c_D=0.01, L_D= 1, r_{wD}=0.0005, s = -1

Table 7: Dimensionless Pressure at Late Dimensionless Time for Different Dimensionless Wellbore Radii, cD= 1, LD = 100, s = 0

t_D	d = 4.5			d = 1.2		
	rwD=0.0001	0.001	0.01	0.0001	0.001	0.01
1	0.0782	0.0552	0.0322	0.0914	0.0684	0.0454
10	0.1012	0.0782	0.0552	0.1145	0.0914	0.0684
100	0.1243	0.1012	0.0782	0.1375	0.1145	0.0914
1000	0.1473	0.1243	0.1012	0.1605	0.1375	0.1145
10000	0.1703	0.1473	0.1243	0.1835	0.1605	0.1375

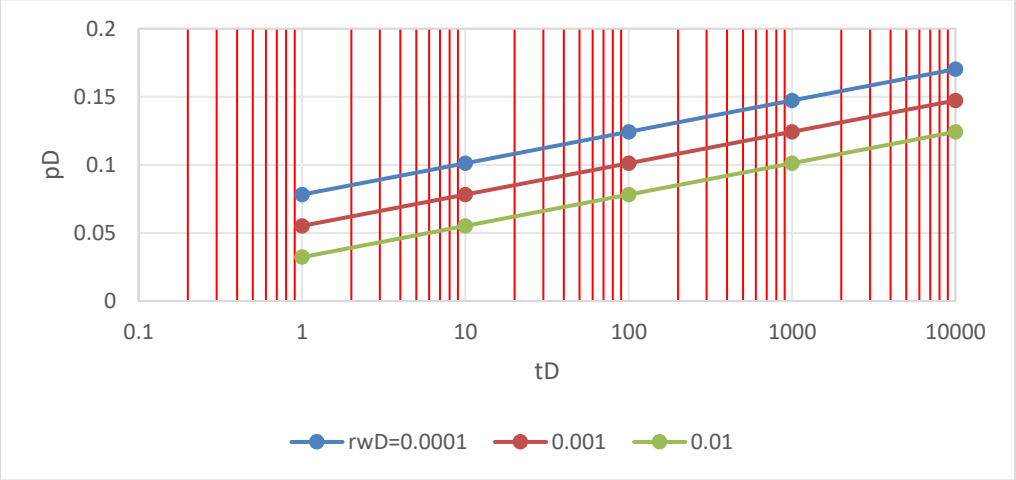

Figure 7: Dimensionless Pressure at Late Dimensionless Time for Different Dimensionless Wellbore Radii, c_D= 1, L_D = 100, s = 0, d = 4.5

Table 8: Dimensionless Pressure at Late Dimensionless Time for Different Dimensionless Wellbore Radii, c_D= 10, L_D = 100, s = 0, d = 4.5

t_D	d = 4.5			d = 1.2		
	r_{wD}=0.0001	0.001	0.01	0.0001	0.001	0.01
1	0.0552	0.0322	0.0091	0.0684	0.0454	0.0224
10	0.0782	0.0552	0.0322	0.0914	0.0684	0.0454
100	0.1012	0.0782	0.0552	0.1145	0.0914	0.0684
1000	0.1243	0.1012	0.0782	0.1375	0.1145	0.0914
10000	0.1473	0.1243	0.1012	0.1605	0.1375	0.1145

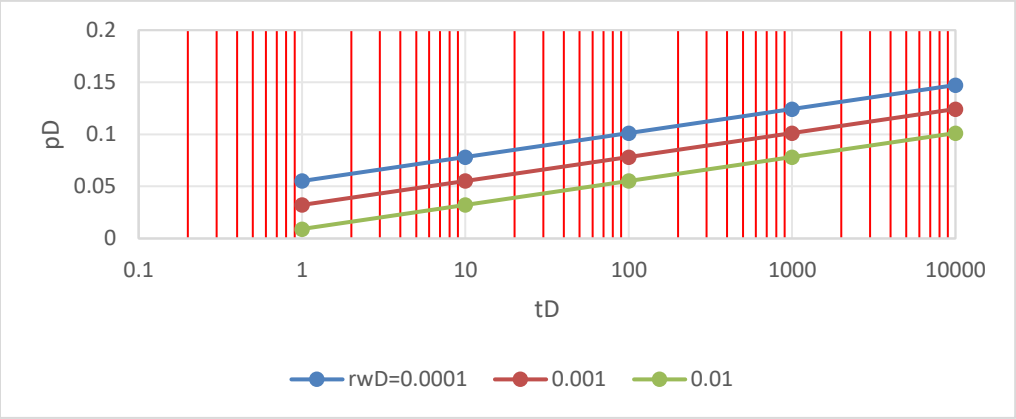

Figure 8: Dimensionless Pressure at Late Dimensionless Time for Different Dimensionless Wellbore Radii, c_D = 10, L_D = 100, s = 0, d = 4.5

Results in Tables 1 to 9, and Figures 2 to 9 show that two (2) characteristic dimensionless pressure gradients are observable. The first and the earlier gradient depicts infinite activity, signifying absence of boundary of any kind. The second slope of 2.3026 per cycle heralds the arrival of a sealing boundary. Results also demonstrate that proximity to a sealing boundary significantly accelerates boundary-dominated flow, steepen pressure derivatives, and increase gradients. Dimensionless derivatives and gradients are strongly affected by dimensionless wellbore radius, boundary proximity and unaffected by skin. Wells located near sealing boundaries display earlier

transitions to boundary-dominated regimes, higher derivatives, and steeper gradients. Conversely, wells farther from boundaries experience prolonged infinite-acting flow and smoother transitions. At early times ($\mathbf{t_D} \leq 0.1$), dimensionless pressures are relatively low and similar at different boundary distances. This reflects the wellbore-dominated flow regime, where boundary effects have not yet influenced the transient behavior. As time increases ($1 \leq \mathbf{t_D} \leq 100$), pressure increases steadily, with noticeable differences based on the dimensionless distance of the well from the sealing boundary. Wells closer to the sealing boundary exhibit earlier attainment of final dimensionless pressure gradients marked as 2.3026 per cycle. At late times, the pressure response tends to stabilize at this dimensionless gradient, indicating transition into the pseudo-steady state regime, where flow is dominated by boundary effects.

Results in Tables 7 and 8 show that, for a fixed object well distance from the boundary, well completion status, well productivity declines with larger dimensionless wellbore radius. Also, well productivity is higher the nearer the wells are from the sealing boundary. When the wells are farther away from the boundary, they seem to exhibit infinite-acting behavior, characterized by lower dimensionless pressure drops, and hence, lower productivity.

The derivative curves shown in Table 9 provide additional diagnostic insight into flow regimes. At very early and late dimensionless flow times, ($t_D \leq 0.1$), all dimensionless pressure derivatives show nearly constant values for all cases considered. At intermediate dimensionless flow times ($1 \leq t_D \leq 100$), the slopes deviate according to boundary distance. For wells close to the boundary ($d = 0.3$), the derivative increases more steeply, consistent with bilinear or linear flow distortion caused by the sealing boundary. At very late dimensionless flow time ($t_D \geq 1000$), the derivatives flatten to a stable value, indicating pseudo-radial flow restricted by the sealing boundary.
The derivative analysis confirms the theoretical expectation that a sealing boundary alters type-curve slopes, leading to boundary-dominated flow. The dimensionless gradients from all results obtained conform to $2.3026/L_D$ per cycle, especially at late dimensionless flow times. Furthermore, since the dimensionless pressure gradient observable per cycle =2.3026, then, according to Reference [9], $2.3026 = 2.3026\alpha/(4L_D)(n+1)$, then, for all L_D, $n = 1$. Also, using dimensionless pressure derivative results, Reference [9] shows that, at late dimensionless time, when the reservoir external boundary is felt, $p'_D = \alpha/(4L_D)(n+1)$. Using $p'_D = 0.9990$ for $L_D = 1$ from Table 9, then, n=1.These results further illustrate the effect of sealing boundaries on horizontal well dimensionless pressures and dimensionless pressure derivative. The gradients increase sharply at early times before stabilizing around a near-constant value. Wells closer to the boundary exhibit higher initial gradients, reflecting stronger flow restriction. At late times ($\mathbf{t_D} \geq 100$), the gradients converge toward a limiting value of approximately 2.3026, consistent with the theoretical pressure gradient.

Table 9: Dimensionless Pressure Derivative for Varying L_D, $c_D = 1$, rwD= 0.001, d = 4.5

t_D	$L_D = 1$	$L_D = 10$	$L_D = 100$
0.01	0.5000	0.0499	0.0050
0.1	0.5000	0.0500	0.0050
1	0.5000	0.0500	0.0050
10	0.5660	0.0566	0.0057
100	0.9083	0.0908	0.0091
1000	0.9900	0.0990	0.0099
10000	0.9990	0.0999	0.0100

CONCLUSION

This research investigated the factors affecting the pressure distribution of a horizontal well near a sealing boundary using dimensionless pressure and dimensionless pressure derivatives distribution. From results obtained, we conclude that

1. The critical factors affecting horizontal well performance are dimensionless wellbore radius, horizontal well length, wellbore skin and storage factor.

2. Boundary proximity plays a critical role in shaping reservoir pressure behaviour. Wells located closer to the sealing boundary experienced larger dimensionless pressure drops, steeper gradients, and earlier boundary effects, whereas those farther away sustained infinite-acting flow for longer before transitioning to boundary-dominated regimes.

3. Sealing boundaries exhibit unique dimensionless gradient of 2.3026 per cycle at late flow time for all well distances from the sealing boundary, and completion status.

4. The dimensionless pressure derivative at late time is constant and dependent inversely on well length.

5. Longer wells extend infinite-acting flow, and extend time external sealing boundary is felt.

6. Slim wellbore will produce significantly swifter flow than thick wells.

7. Wellbore skin does not affect horizontal well dimensionless pressure gradients and dimensionless pressure derivatives at all flow late flow times.

Nomenclature

d=dimensionless distance from well to boundary

s=Skin factor

$\alpha = 2$

OW = Object horizontal well

IW = Image horizontal well

L_D=Dimensionless length of horizontal well

Ei=Exponential integral function ,

r_{wD}= Dimensionless wellbore radius

t_D=Dimensionless time

c_D= Dimensionless wellbore storage coefficient

$_P$D= Dimensionless Pressure

$_P$D`= Dimensionless pressure derivative

REFERENCES

1. Adewole, O., and Orene, P. (2018). *Horizontal well performance near sealing boundaries*. Journal of Petroleum Science, 45(3), 221–234.

2. Daviau, F. Mouronval, G. Bourdarot, G. and Curutchet, P.(1988). Pressure Analysis for Horizontal Wells, *SPERE*, 716 - 724, *Trans*., AIME, 285.

3. Earlougher, R.C.Jr. (1977) *Advances in Well Test Analysis*,SPE Monograph Series, (5), 124.

4. Gringarten, A. and Ramey, H. J. (1973) The Use of Source and Green's Functions in Solving Unsteady-Flow Problems in Reservoirs; *SPEJ*, October, 285 – 296.

5. Kitungu, P., Mutinda, J., & Wambua, D. (2025). Well test interpretation of horizontal wells in bounded anisotropic reservoirs. *Petroleum Systems and Reservoirs*, *15*(2), 88–101.

6. Ozkan, E., and Raghavan, R. (2000). Pressure-transient behavior of horizontal wells. *SPE Journal*, *5*(3), 259–268.

7. Ozkan, E., Raghavan, R., & Joshi, S. (2021). Pressure-transient analysis of horizontal wells revisited. *SPE Reservoir Evaluation & Engineering*, *24*(2), 214–228.

8. Zhang, L., Chen, Q., & Hu, Z. (2021). Fault sealing effects on horizontal well performance. *Petroleum Exploration and Development*, *48*(6), 1345–1356.

9. Atasie, B.C., Ana, E.A. and **Adewole, E.S.** "Characteristics of a Horizontal Well Completed Within a Pair of Inclined Sealing Oil Reservoir Boundaries" *Journal of Engineering for Development*, Vol. 17(3), September (2025) pp.13 - 21, https://jedev.com.ng/